



A review on metallic porous materials: pore formation, mechanical properties, and their applications

Biao Zhao¹ · Asit Kumar Gain² · Wenfeng Ding¹ · Liangchi Zhang² · Xianying Li¹ · Yucan Fu¹

Received: 12 July 2017 / Accepted: 14 November 2017 / Published online: 25 November 2017
© Springer-Verlag London Ltd., part of Springer Nature 2017

Abstract

This paper presents a comprehensive review on the mechanism of pore formation, mechanical properties, and applications of metallic porous materials. The different manufacturing techniques of metallic porous materials using various pore-forming agents (e.g., sodium chloride, polymethyl methacrylate, magnesium, and cenosphere) are highlighted in the first part of this review. Subsequently, the pore formation mechanism and pore morphology in final products as well as corresponding pore-forming agent removal techniques (e.g., sintering-dissolution process, thermally stimulated decomposition, thermally melted elimination, and embedding cenosphere technique) are specifically discussed. Then, some major influential factors on the mechanism of pore formation, including pore size, shape, distribution, and porosity, are analyzed in detail. Meanwhile, the primary mechanical properties such as compressive strength, elastic modulus, fatigue properties, and flexural strength of metallic porous materials depending on pore morphology and porosity are explored in detail. Furthermore, their applications in structural and functional aspects according to their pore morphology and mechanical properties are emphatically summarized. Finally, this review article highlights some important factors for advanced wear-resistant tool and biomedical implant applications of porous metallic materials.

Keywords Metallic porous materials · Pore-forming agents · Fabrication technology · Mechanical property · Application

1 Introduction

The discovery of microporous/mesoporous materials has opened up great opportunities in industrial applications. However, the applications of porous materials (typically highly porosity) and metal foams (metals with pore deliberately integrated into their structure) depends on their physical and mechanical properties [1]. For example, closed cell porous materials having higher mechanical properties are mainly used in structural applications. On the other hand, opened cell porous structure materials which contain interconnected porous

structure as well as poor mechanical properties are mainly used in functional applications. Generally, metallic porous materials are widely used in wear-resistant tools, biomedical implants, catalyst, and heat exchangers because of their exceptional physical properties such as high gas and liquid permeability, high strength-to-weight ratio, low density, and excellent energy absorption characteristics [2–4]. Various fabricating processes have been developed to manufacture the metallic porous materials. The mainly research methods include sol-gel, polymer porosifier method, foaming method pore-forming agent/space holder method, and additive manufacturing (AM) techniques [5–11]. Among the above processes, the fabrication techniques, e.g., space holder method and additive manufacturing (AM) have been widely used to manufacture the metallic porous materials without contamination. Undoubtedly, the porosity and pore morphology of metallic porous materials depends on several factors for example types of pore-forming agents (e.g., sodium chloride, polymethyl methacrylate, magnesium and cenosphere) volume percentage, size, and shape, and sintering process. Furthermore, the porosity and pore morphology strongly influence on the structure and/or mechanical properties of metallic porous materials [12–15].

✉ Wenfeng Ding
dingwf2000@vip.163.com

✉ Liangchi Zhang
liangchi.zhang@unsw.edu.au

¹ College of Mechanical and Electrical Engineering, Nanjing University of Aeronautics and Astronautics, Nanjing 210016, People's Republic of China

² Laboratory for Precision and Nano Processing Technologies, School of Mechanical and Manufacturing Engineering, The University of New South Wales, Kensington, NSW 2052, Australia

With respect to their origin and structure, the pores in final structures can be divided into two categories, (1) the inherent pores (without pore-forming agents) and (2) the generated pores (with pore-forming agents). Generally, this inherent mesoporous structure is the intrinsic characteristics of powder metallurgy products, which is mainly formed due to the particles size, distribution and density of starting powders [16]. On the other hand, the different mixtures of raw materials and pore-forming agents are cold pressed to form composite blocks prior to sintering and then the generated pores are introduced in the final products after thermal processing (sintering or solidification of metallic melts) by employing various pore-forming agents. Generally, the generated porosity of metallic materials can be classified into two categories, which are open porosity and closed porosity, depending on the connectivity of the pores [17]. Open porosity as the typical representative in final structure of porous materials is mainly obtained after burning out the pore-forming agents or removing the leachable preforms. Along this line of consideration, the porous materials with closed porosity are fabricated by adding the preliminary-obtained cenospheres (e.g., alumina bubble particles) to mixed powders before thermal processing and then the closed pores resulted from cenospheres are obtained in sintered metallic porous materials. In addition, the pore morphology (size, shape and porosity) in the final sintered bodies depends on the type, size and volume percentage of pore-forming agents as well as the removal processes of pore-forming agents [18]. Particularly, the removal and manufacturing processes depends on the types of pore-forming agents and affects the physical and mechanical properties of metallic porous materials to an extent. Furthermore, the porous materials having same apparent porosity but the different pores size and shape react in a different way under the same conditions. Therefore, the “pore size” is a property of major importance in practical applications of porous materials, but it is even less susceptible to precise definition [19]. According to the relative pore size in basic structural elements of the porous material, they could be classified into four types and defined as follows: (i) macropores ($r > 1000$ nm)—are specified as pores with size considerably higher than individual element size; (ii) micropores ($100 < r < 1000$ nm)—are pores with approximately the same size as the structural elements; (iii) submicropores ($r < 100$ nm)—have pores that are considerably smaller than structural particles; and (iv) ultramicropores ($r < 1\div 2$ nm)—could be found inside structured elements [19, 20].

This article aims to provide a review on the manufacturing process of metallic porous materials, mechanical properties evaluation and their advanced industrial applications. The pore morphologies, e.g., size, shape, porosity, and connectivity are discussed depending on the manufacturing process and nature of the pore-forming agents. In addition, their mechanical properties primarily, e.g., compressive strength, fatigue properties

elastic modulus and flexural strength, and their structural applications (e.g., wear-resistant tools and biomedical implants) and functional applications (e.g., catalyst and heat exchangers) are specifically discussed in detail. For an easy understanding of the fabrication techniques for metallic porous materials, a summarized flowchart is firstly demonstrated in Fig. 1.

2 Mechanism of pore formation and fabrication technology of metallic porous materials

Techniques for fabricating metallic porous materials provide various pore structures; depending on their applications, it is possible to obtain porous structures with various pore size, shape and distribution. In methods of phase separation techniques (e.g., sintering-dissolution process, thermally stimulated decomposition, and thermally melted elimination) and embedding cenosphere technique primarily elaborated as follows, the porosity and mechanical properties can be effectively controlled by altering the volume percentage and size of the pore-forming agents. In the phase separation technique, the various pores appear owing to temperature changes and removal processes to achieve the removal of pore-forming agents, which are always tiny and irregular. In case of embedding technique, the porosity is tailored by the amount and size of the embedded preliminary-obtained cenosphere particles, leaving closed pores in the final structure. On the other hand, in advanced additive manufacturing (AM) technique, the continuous porous materials are manufactured using layer-by-layer deposition through high-energy electron beam melting (EBM) and selected laser sintering (SLS) processes.

2.1 Sintering-dissolution process

The various pore-forming agents (e.g., sodium chloride, carbamide, and saccharose) offering peculiar properties, such as water-soluble, non-toxic, low-cost, and high melting points, make them a considerable removable additive by applying sintering-dissolution process (SDP). It was worthy noted that these additives dissolve in water from the green bodies prior to sintering and generated pores in the final products [21]. Moreover, processing parameters (e.g., pore size, sintering parameters) of SDP have a significant effect on the porosity and physical properties of the porous material [22–24]. The flowchart for operations of SDP technology is visualized in Fig. 2.

Among the water-soluble pore-forming agents, sodium chloride (NaCl) particles have been considered a suitable pore-forming agent to fabricate the porous materials, due to their good inherent physical properties such as solubility, high melting points, non-toxic, and low cost. However, the corrosion may take place with the NaCl particles left in final structure without sufficiently dissolution. Therefore, the machining

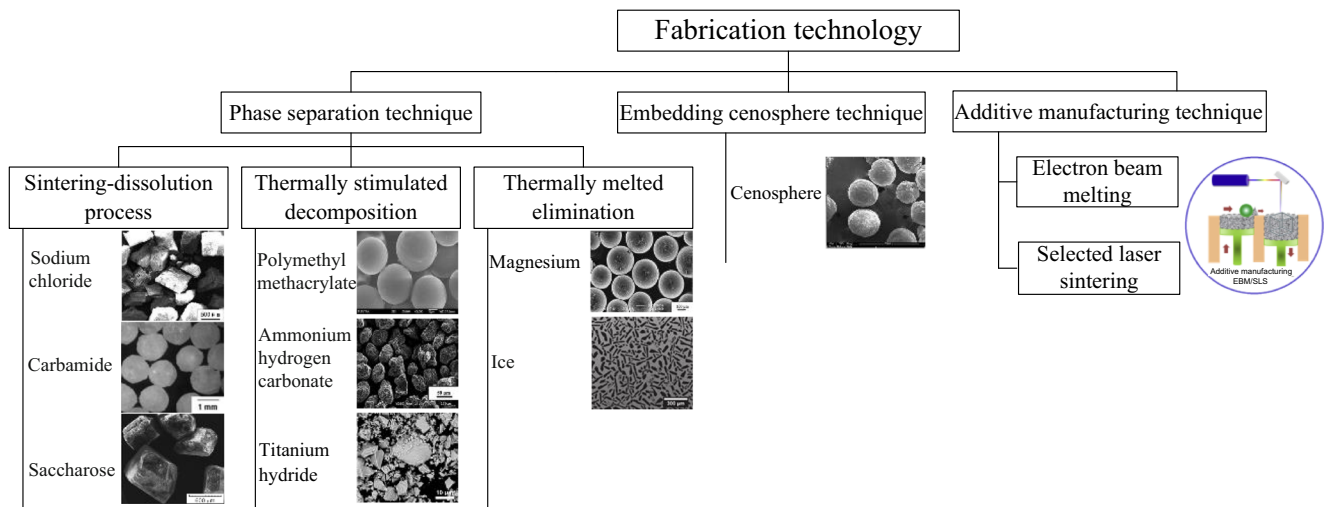


Fig. 1 Flowchart of fabrication techniques for metallic porous materials

performance of porous materials would be affected by the pore-forming NaCl particles size, distribution, concentrate and dissolution technique (Table 1, 1–4). Wang et al. [21] used NaCl particles to fabricate an opened cell porous Cu material with 71.3% porosity by using SDP primarily. The study showed that the optimized compaction pressure and sintering temperature were 250–300 MPa and 940–960 °C, respectively. Golabgir et al. [22] also manufactured an opened cell porous Fe-Al materials (having porosity about 65%) by adding the pore-forming NaCl particles and polyester resin (binder) through the sintering-dissolution process. They reported that the oxidation resistance of opened cell porous Fe-Al materials improved as increasing the sintering temperature and dissolution time. Jha et al. [23] manufactured the opened cell porous titanium materials with 65–80% porosity using NaCl particles as temporary pore-forming agents. They found that the pore-forming agents were successfully removed from the final products through the hot water treatment after sintering. Furthermore, Zhao et al. [24] investigated the pores structure and formation mechanism of high porosity NiTi alloys (having porosity approximate 90%) fabricated by powder metallurgy technique using raw powders of Ti, Ni and pore-forming NaCl particles. Their findings indicated that the porosity was increased linearly with the volume percentage of NaCl particles under the same forming pressure and sintering process in a vacuum furnace at 950 °C for 2 h.

Similarly, carbamide ((NH₂)₂CO) has also been recognized a suitable water-soluble pore-forming agents for developing metallic porous materials as presented in Table 1 (5–6). Bakan [25] proposed a novel water leaching and sintering process to fabricate stainless steels with 70% porosity by using irregular (NH₂)₂CO particles as pore-forming agents. The results from the detection of the macro-pore structure revealed that the pore shape, size and distribution could be tailored with this above process. Bafti and Habibolahzadeh [26] evaluated the effect of processing parameters (e.g., applied pressure, dissolving time of spacer, sintering temperature, and time) and additives structure (e.g., pore size, shape, and distribution), on the microstructure of aluminum porous materials with 40–85% porosity via power-(NH₂)₂CO space route. They found that the ideal morphology of porous materials were obtained using spherical-shaped (NH₂)₂CO particles.

Saccharose (C₁₂H₂₂O₁₁) is a considerable potential and non-toxic material, easy to fabricate a structural material as pore-forming agents (Table 1, 7–8). Michailidis et al. [27] fabricated the porous aluminum materials with porosities (50–75%) via powder metallurgy using a leachable pore-forming agent of C₁₂H₂₂O₁₁ particles. The findings suggested that good reproducibility was achieved especially in porous materials with small pore size. The porous titanium composites of designed porosity (approximately 50–70%) were fabricated by adding spherical and polyhedral-shaped C₁₂H₂₂O₁₁

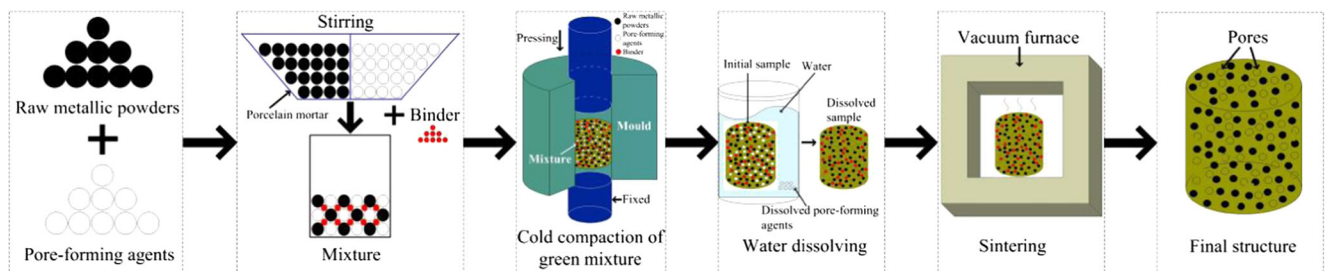
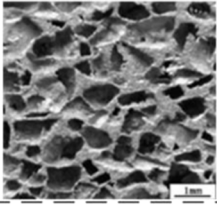
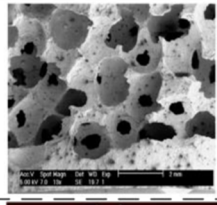
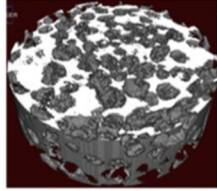


Fig. 2 Flowchart for operations of sintering-dissolution process technology

Table 1 Various pore-forming agents used in foam fabrication by sintering-dissolution process.

Technique	No.	Raw materials	Pore-forming agents	Porosity [%]	Pore size [μm]	Morphology (porous composites)	
Sintering-dissolution process	1	Cu [21]		71.3	750		
	2	Fe(Al) [22]	Sodium chloride (NaCl)	65	200–500		
	3	Titanium [23]		65–80	230 \pm 2		
	4	Ni-Ti [24]		90	200–400		
	5	Stainless steel [25]	Aluminum [26]	Carbamide ((NH ₂) ₂ CO)	70	750–1000	
	6				40–85	1000–5000	
	7	Aluminum [27]	Titanium [28]	Saccharose (C ₁₂ H ₂₂ O ₁₁)	50–75	125–2000	
	8				50–70	700–900	

particles and then their morphology was investigated by Jakubowicz et al. [28]. The results from the microstructure and morphology revealed that the porous titanium composites fabricated with 100 mesh Ti powder and spherical-shaped C₁₂H₂₂O₁₁ particles was related to better sintering compared with 325 mesh Ti powders and polyhedral-shaped C₁₂H₂₂O₁₁ particles.

2.2 Thermally stimulated decomposition

There are some published reports on the studies of metallic porous materials with various space holder additives, such as polymethyl methacrylate (PMMA) (Table 2, 1–2) [29, 30], ammonium hydrogen carbonate (NH₄HCO₃) (Table 2, 3) [31], titanium hydride (TiH₂) (Table 2, 4–5) [32, 33], exhibiting pyrolysis, non-toxic and non-contamination for metal powders. Generally, these low melting point volatile materials are thermally decomposed during the heat treatment process and initiated irregular-shaped pores in the sintered bodies as shown in Fig. 3. Briefly on this process, the mixer of low melting point volatile pore-forming agents and raw matrix powders compacted at room temperature to make green bodies and then the pore-forming agents burn-out during sintering process and leave a porous structure. Through an even dispersion of powder mixture a uniform distribution of pores (often with random shape) are achievable [34]. However, the heating rate during the burning out process for removing the volatile pore-forming agents is quite important

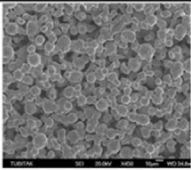
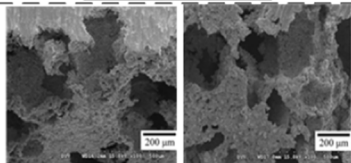
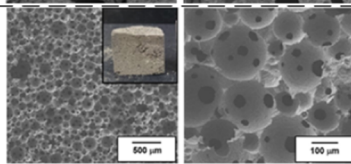
to avoid the processing defects such as swelling, delamination and cracks.

Gülsoy and German [29] investigated the production of microporous austenitic stainless steel 316L (having porosity approximately 40–60%) with polymethyl methacrylate (PMMA) decomposed easily during sintering process. Findings were that the raw materials exhibited excellent mouldability and no separation of the binder was observed. Furthermore, the increases in the volume fraction and average size of PMMA in a range of 10–40 μm led to decrease the elastic modulus and the density of sintered bodies. Xie et al. [30] studied the mechanism of pore formation of microporous aluminum materials with high porosity fabricated with a mixer of aluminum powders and PMMA particles. The results showed that the pores in final structure could be controlled by varying the size of pore-forming agents PMMA powders.

Hsu et al. [31] fabricated the porous Ti-7.5Mo alloys with pore sizes of approximately 0.15–0.6 mm via powder metallurgy based sintering process (at 1100 °C for 10, 15, and 20 h, respectively) using Ti and Mo raw powders and 60 vol.% of a thermolabile pore-forming agent ammonium hydrogen carbonate (NH₄HCO₃) powders. A positive correlation between the relative density of the specimens and sintering times was obtained.

Luo et al. [32] evaluated the decomposition behavior of titanium hydride (TiH₂) powders as the blowing agent employed to fabricate porous aluminum materials. The heat treatment process for TiH₂ at 500 C between 1 and 5 h in air was found to be the most favorable method to manufacture

Table 2 Various pore-forming agents used in foam fabrication by thermally stimulated decomposition technology.

Technique	No.	Raw materials	Pore-forming agents	Porosity [%]	Pore size [μm]	Morphology (porous composites)
Thermally stimulated decomposition	1	Stainless steel [29]	Polymethyl methacrylate (PMMA)	40–60	10–40	
	2	Aluminum [30]		5–50	20–50	
	3	Ti–7.5Mo alloy [31]	Ammonium hydrogen carbonate (NH_4HCO_3)	—	150–600	
	4	Titanium [32]	Titanium hydride (TiH_2)	—	125–2000	
	5	Titanium [33]		82 ± 1.3	150 ± 65	

porous aluminum materials. In addition, Ahn et al. [33] produced highly porous titanium materials ($82 \pm 1.3 \text{ vol.}\%$) with large interconnected pores using vacuum-assisted processing. A good shape tolerance with a uniform porous structure was shown both with and without vacuum-assisted processing.

2.3 Thermally melted elimination

The thermally melted additives (e.g., magnesium (Table 3, 1) [35] and ice (Table 3, 2) [36]) are also successfully used as pore-forming agents to fabricate metallic porous materials. These pore-forming agents melt during the sintering process. The flowchart for operations of thermally melted elimination process is visualized in Fig. 4.

Aşik and Bor [35] studied the fatigue behavior of porous Ti-6Al-4V materials fabricated via powder metallurgy process, where spherical magnesium powders were utilized to produce the highly porosities (51–65%) and large size pores (approximately $375 \mu\text{m}$) using magnesium as a vaporizable pore-forming agent sintered at $1200 \text{ }^\circ\text{C}$ for 2 h. The final structure was composed with spherical, interconnected and

irregular-shaped micropores. However, the porous titanium alloys with elongated-shaped pores were fabricated by Chino and Dunand [36] using the directional freeze casting (DFC) technique due to the removal of ice dendrites after freeze-drying processes. Signs of embrittlement were emerged in sintered structures owing to the high powder oxygen content.

2.4 Embedding cenosphere process

Owing to the relatively high melting point, the embedded preliminary-obtained Cenosphere particles as pore-forming agents in the metal matrix are not thermally decomposed or melted during the sintering process; thus, the closed pores appear in final structures (Table 4) [37–39]. Figure 5 visualizes the flowchart for operations of embedding cenosphere process.

Guo and Rohatgi [37] initially fabricated and evaluated aluminum cenospheres composites with cenospheres as reinforcements via powder metallurgy techniques. An appropriate pressure parameter was found to produce metal matrix

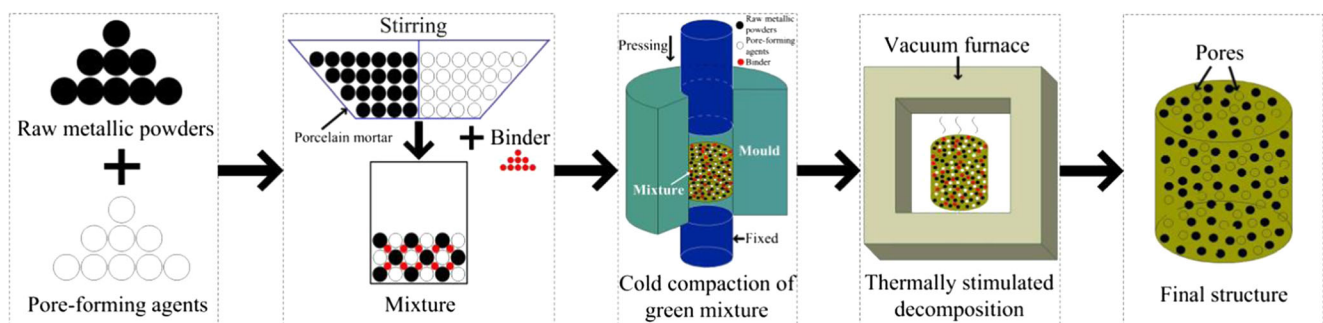
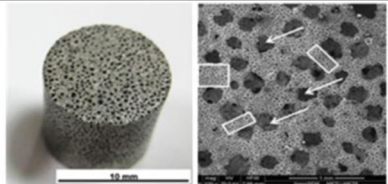
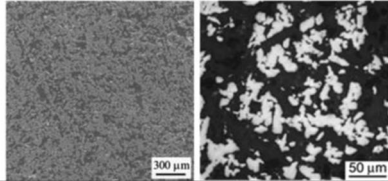
**Fig. 3** Flowchart for operations of thermally stimulated decomposition technology

Table 3 Various pore-forming agents used in foam fabrication by thermally melted elimination technology.

Technique	No.	Raw materials	Pore-forming agents	Porosity [%]	Pore size [μm]	Morphology (porous composites)
Thermally melted elimination	1	Ti-6Al-4V [35]	Magnesium (Mg)	51–65	375	
	2	Titanium [36]	Ice	57–67	50–170	

syntactic foams. Furthermore, Rheinheimer et al. [38] fabricated ultra-light weight cement composites with closed pores using hollow cenosphere particles as pore-forming agents and established the composite model to analyze the homogenization of the hollow spheres. A good consistency between the numerical simulation and the measured data was achieved. Meanwhile, Vogiatzis and Skolianos [39] evaluated the sintering mechanisms and microstructure of porous metal matrix materials embedded with ceramic cenospheres (10–40 vol.%) through powder metallurgy route. A relative homogeneous distribution of the cenospheres was observed with limited clustering especially at low temperatures (610 °C)

2.5 Additive manufacturing

Recently, additive manufacturing technique plays an important role to manufacture the near-net-shape complex dense or porous part with tailored mechanical properties for biomedical and aerospace applications. In this process, complex-shaped parts are manufactured from the computer aided design (CAD) by the addition of metal layer by layer through an electron beam melting (EBM) or a direct metal laser sintering (DMLS) techniques [40–42]. To briefly explain this manufacturing process, a high-energy electron beam or a high-power laser is scanned on the metal powder surface

and sintered a thin metal layer according to CAD models. After completing the first layer, a new layer of material is deposited on the top and this process is repeated until the desired shaped part is completed according to Fig. 6.

3 Mechanical properties of metallic porous materials

For metallic porous materials, the evaluation of mechanical properties including compressive strength, fatigue behavior, elastic modulus, and flexural properties is the critical factors for specific industrial applications. Similar to the situation with the mechanism of pore formation and fabrication technology, these properties have been studied variously in the breadth and depth of the reported literature. Furthermore, the parametric studies with the sintering process, porosity and fabrication technology have received the most attention, which is dependent on the evaluation of these properties reflecting the integrality performance of metallic porous materials. Therefore, the fine control of pore characteristics of metallic porous materials and resulting mechanical behavior is worth studying to achieve the design requirements for a specific application.

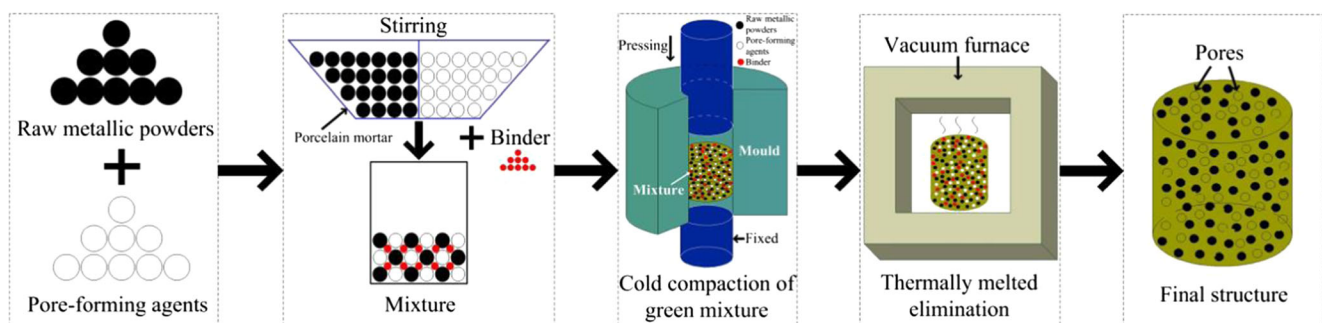
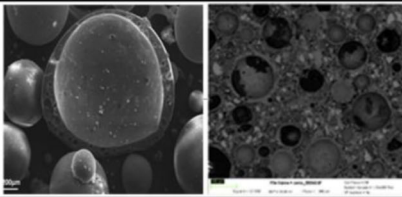
**Fig. 4** Flowchart for operations of thermally melted elimination technology

Table 4 Various pore-forming agents used in foam fabrication by embedding cenosphere process

Technique	No.	Raw materials	Pore-forming agents	Porosity [%]	Pore size [μm]	Morphology (porous composites)
Embedding cenosphere process	1	Aluminum [37]		–	50–150	
	2	Ultra-lightweight composites [38]	Cenosphere	57–67	10–300	
	3	Aluminum [39]		10–40	10–150	

3.1 Compressive properties

Generally, the mechanical property of metallic porous materials under compressive loads is significantly influenced with the internal architecture as well as porosity [43, 44]. A bulk of theoretical and experimental studies have been reported regarding compressive strength dependence on structural variations. The compressive strength of metallic porous materials with various fabrication technologies are given in Table 5. Jiang et al. [45] evaluated the physical properties and compressive properties of porous aluminum materials with high porosity (approximate 70%) synthesized with different shapes of the carbamide particles. The measurement results suggested that a higher compressive strength was obtained with spherical-shaped pore-forming agents than that of manufacture with strip-shaped pore-forming agents. Nieh et al. [46] investigated the influence of pore morphology on compressive strength of opened cell porous aluminum materials. Their study confirmed that the pore shapes of porous metallic materials were greatly influenced on their mechanical properties as compared to their pore size. Furthermore, Bafti and Habibolahzadeh [47] reported that angular carbamide particles significantly reduced mechanical properties and then the desired compressive strength of porous aluminum material were obtained via employing the spherical-shaped pore-forming particles. For porous titanium materials, Imwinkelried [48] studied the mechanical properties of titanium materials with porosities (50–80%) via powder metallurgy by employing nonspherical-shaped ammonium hydrogen carbonate (NH_4HCO_3) particles as pore-forming agents. A

weaker structure along the compaction direction was observed owing to the uniaxial pressing. Tuncer et al. [49] investigated the influence of pore aspect ratio on the structure and compressive strength of porous titanium materials with spherical, angular, and needle-like carbamide particles. According to the Fig. 7, an approximately reverse tendency was given between average aspect ratio pores and compressive strength, irrespective of the porosity and then the decline of compressive strength could be avoided by adding low aspect ratio particles, that is, spherical-shaped particles.

In addition, the effect of porosity of porous Ti-10Mo alloy manufactured using NH_4HCO_3 as pore-forming agents on the compressive strength and elastic modulus was elaborately studied by Gao et al. [50]. The porosity of this material increased as increasing the volume percentage of pore-forming agents NH_4HCO_3 particles. The porosity of this material has proven to be the main influences on a sustained decline in the compressive strength and elastic modulus. Wang et al. [51] investigated the compressive strength and deformation mechanism of the porous copper materials by employing pore-forming agents NaCl particles under quasi-static compressive condition. The stress-strain curves showed a slight dependence on strain rate at high strain levels in densification stage. Moreover, the phenomenon of the layer-by-layer collapse was observed due to the high stress, which revealed the predominant deformation mechanism of opened cell porous copper alloys. Nakaş et al. [52] studied the influence of porosity on the compressive strength of porous TiNi materials using spherical-shaped magnesium powders with average size of 450 μm . The continuous decline in compressive strength

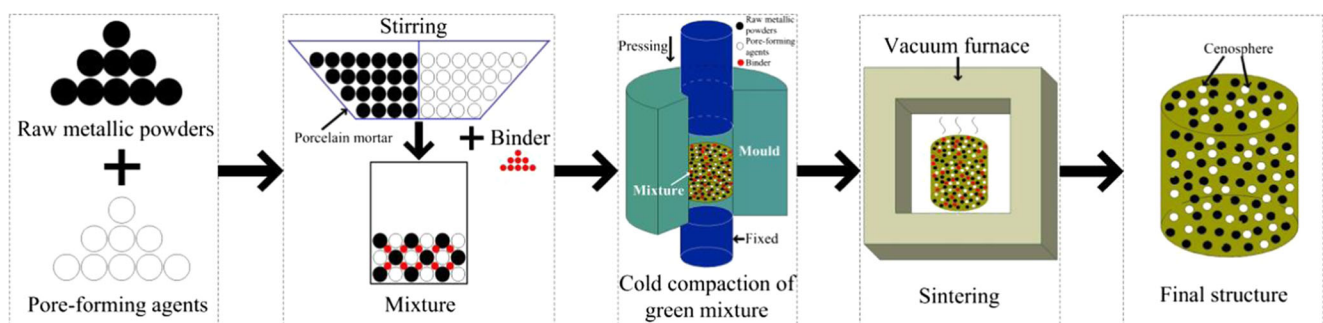
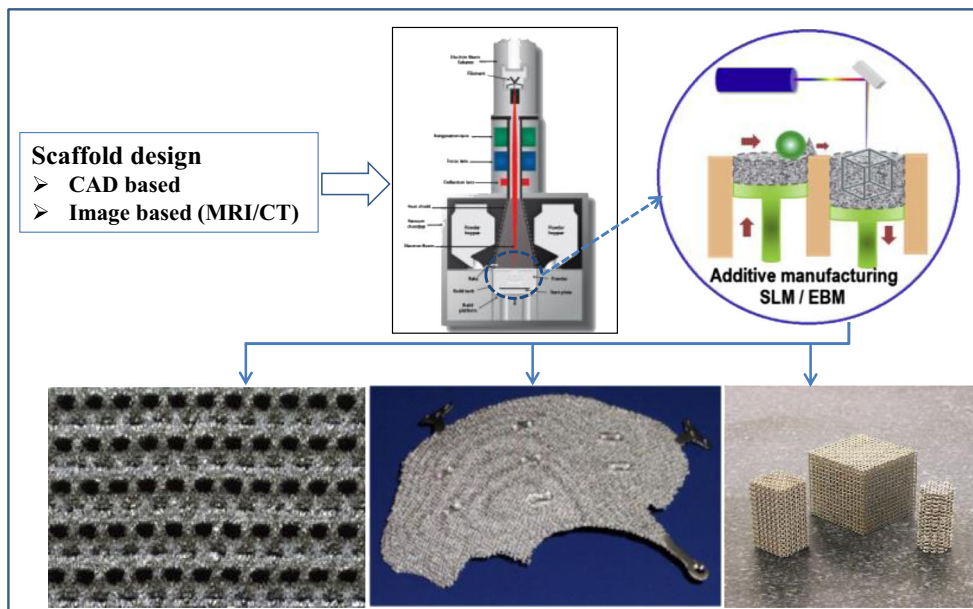
**Fig. 5** Flowchart for operations of embedding cenosphere process

Fig. 6 Additive manufacturing process for near-net-shape metallic porous materials [40–42]



and elastic modulus was revealed due to an increase in porosity. Li and Dunand [53] evaluated the mechanical properties of porous titanium materials with aligned pores using DFC technology of aqueous slurries of titanium powders, followed by ice sublimation and powder sintering. The semi-ductile behavior and high-energy absorption of porous titanium materials appeared under compressive loads. Sankaranarayanan et al. [54] evaluated the effect of cenosphere particles on the compressive behaviors of porous magnesium materials. Their

experimental results showed a slight improvement in compressive strengths of porous magnesium materials by employing cenosphere particles as pore-forming agents. Vogiatzis et al. [55] proposed a new mathematical model to predict the compressive strength of porous aluminum-ceramic cenospheres materials. The relative error between the experimental and theoretical magnitude calculated by Eq. (1) as follows appeared at 15% below without considering the influence of cenospheres fragments numerically.

$$\sigma_{cth} = C \times \left(\frac{P_c}{3 \left(\ln \left(\frac{1}{1-\rho_{sf}} \right) - A \right)} \times (1-V_{ceno})^{3/2} + \sigma_{wall} \times V_{ceno} \times \left(1 - \left(1 - \frac{t}{R} \right)^3 \right)^{3/2} \right) \tag{1}$$

where σ_{cth} was the estimated compressive strength and C a constant assumed equal to 0.3. P_c and ρ_{sf} were the relative density of the compact green body and the examined materials, respectively. A was constant equal to 0.9, σ_{wall} the compressive strength of the wall material of the cenospheres, and V_{ceno} the volume fraction of cenospheres. t is the wall thickness and R is the radius of the cenospheres.

3.2 Elastic modulus

Recently, porous metallic artificial implant plays an important role for load-bearing parts. However, for load-bearing implant applications, the evaluation of elastic behavior of porous materials is one of the critical factors because of their

mismatching elastic properties with human cortical bones as presented in Table 6 [56].

Our previous studies have confirmed that highly porous materials significantly decrease the elastic modulus and compressive strength [13, 34]. Niu et al. [57] developed a classical equation between the elastic modulus and relative density of porous materials and expressed as follows:

$$E/E_s = \rho/\rho_s \tag{2}$$

$$\sigma_{pl}/\sigma_{ys} = 0.3(\rho/\rho_s)^{3/2} \tag{3}$$

where E is the elastic modulus of porous materials, E_s is the elastic modulus of the cell edge solid material, σ_{ys} is the yield strength of the cell edge solid material porous materials, and σ_{pl} is the plateau stress of the of porous materials.

Table 5 Compressive behaviors of metallic porous materials with various fabrication technologies

No. technique	Raw materials	Pore-forming agents	Porosity [vol%]	Pore shape	Compressive strength (MPa)	Elastic modulus (GPa)
1 Sintering-dissolution process	Titanium [49]	Carbamide	44	Spherical	185	–
				Angular	175	
				Needle-like	140	
2 Thermally stimulated decomposition	Titanium [43] Ti-15Mo [53]	NH ₄ HCO ₃	78 7.9 29.7 62.5	Spherical	35	5.3
				Spherical	1166	49.2
					360	25.6
					82	4.6
3 Thermally melted elimination	TiNi [52]	Magnesium	49 58 64	Spherical	273.45 ± 9.25	8.71 ± 0.24
					174.75 ± 10.75	5.87 ± 0.31
					93.27 ± 5.30	2.93 ± 0.03
4 Embedding cenosphere process	Magnesium [54]	Cenosphere	13.24 26.48 39.72	Spherical	45.0 ± 2.1	218 ± 8
					42.9 ± 1.6	226 ± 11
					43.1 ± 1.8	221 ± 7

3.3 Fatigue properties

On account of the structural characteristics of metallic porous materials used in an increasing range of applications, especially in load-bearing orthopedic implants and automobile field, the fatigue behavior under service should be investigated. Particularly, porous titanium alloys have been recognized as a suitable candidate for prostheses or dental implants because of their biocompatibility with tissue among several other options (e.g., porous aluminum or cuprum alloys). To ensure ingrowth of tissue, the formation and fatigue crack growth resulted from the response to the repeated cyclic loading should be investigated, which seriously affects its service life [58]. As has already been stated, the structural and functional fatigue of porous Ni-Ti alloys under cyclic loading was evaluated by Eggeler et al. [59]. The structural fatigue was found to be depended on the occurrence and development of surface cracks and the functional fatigue was closely related to the increase in the inner residual strain. Meanwhile, Lin et al.

[60] investigated the microstructure and fatigue properties of porous Ti35Nb alloy under cyclic loading. The recorded value of fatigue limits were displayed as 15.12 MPa at 10⁷ cycles (Table 7, 1). In addition, the fatigue cracks was tended to appear on the wall of micropores and developed along this wall. Eventually, the fatigue cracks of porous Ti35Nb alloy were visualized due to the redundant load transferred by the failure of adjacent struts. Similarly, Nakaş et al. [52] evaluated the fatigue behavior of porous Ni-Ti alloys fabricated with magnesium particles as pore-forming agents under cyclic loading. The value of fatigue limit was found approximately to be 60% of yield strength, which was irrelevant to the porosity (Table 7, 3). In addition, the fatigue fracture was detected owing to the formation of coalescence of microcracks on the pore surfaces due to the development of the macro-cracks on the pore walls. Meanwhile, the obvious crack was aligned at 45° to the loading direction.

Furthermore, the construction components of vehicles are also evaluated the fatigue behavior owing to the frequent vibrations and repeated mechanical straining. Zettle et al. [61] studied the fatigue properties of porous aluminum materials

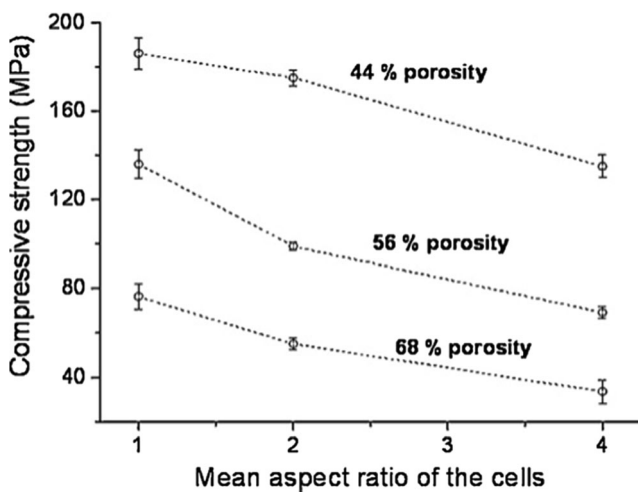


Fig. 7 Compressive strength evolution with aspect ratio of the produced porous titanium materials at three different porosity levels [49]

Table 6 Elastic modulus and porosity of metallic materials [56]

Material	No.	Porosity [%]	Elastic modulus [GPa]
Bone	1	5–90	0.1–30
Dense Ti	2	0	80–130
Porous Ti	3	78	5.3
Porous Ti6Ta4Sn	4	75	4.6
Porous Ti NbSn	5	30–60	10.8–33.2
Porous Ti10 Nb10Zr	6	59	5.6
Porous TiZr	7	70	15.3
Porous Ti15Mo5 Zr3Al	8	26	20
Dense Ta	9	0	185
Porous Ta	10	75–85	2.5–3.9

Table 7 Fatigue behaviors of metallic porous materials

No.	Raw materials	Pore-forming agents	Porosity [vol%]	Applied load type	Frequency (Hz)	Compressive strength (MPa)	Run-out (cycles)
1	Ti-35Nb [60]	NH ₄ HCO ₃	66	Compression-compression	10	10.15	10 ⁷
2	Aluminum [61]	TiH ₂	–	Tension-compression	5	1.1–1.4	10 ⁹
3	Ti-Ni [52]	Magnesium	49	Compression-compression	5	88.76	10 ⁶
			58			54.90	
			64			26.47	

under fully reversed loading conditions. The fatigue limit was about 1.1–1.4 MPa at 10⁹ cycles under fully reversed tension-compression loading [Table 7 (2)]. Meanwhile, the initial defects (e.g., precracks, holes) in the interior structure of pores are likely to generate the initial cracks and the fatigue fracture appears preferentially in areas with low material density or large pores. The fatigue crack was also preferentially developed on thin walls of micropores, and eventually developed along this wall.

3.4 Flexural properties

For the flexural properties of metallic porous materials, only a few parametric investigations have been reported. As has already been stated, the flexural property is largely dependent on the magnitude of porosity and inhomogeneity of metallic porous materials. Imwinkelried [48] evaluated the flexural properties of porous titanium materials (50–80%) with NH₄HCO₃ particles as pore-forming agents using three point bending test. The flexural strength of the 3-point bending tests was calculated by Eq. (2). Results suggested that the maximum flexural stress was closely correlated with the porosity. In addition, the combination of various failure types on the pore walls (e.g., bucking, bending, and tearing) was observed on the fracture morphology. Similarly, Amigó et al. [62] used NH₄HCO₃ particles as pore-forming agents to fabricate the porous TiCP3 materials with porosities (35–80%) and studied their flexural properties. A higher flexural strength is obtained by employing smaller size and lower volume percentage of pore-forming agents NH₄HCO₃ particles. For closed-pore metallic alloys, Ma et al. [63] conducted the 3-point bending tests for porous Cu-Sn-Ti alumina composites (having porosity 20–50%) by employing alumina bubble particles. Their results confirmed that the flexural strength could be tailored by altering the size and concentration of alumina bubble particles.

$$\sigma_{\max} = \frac{3FL}{2bh^2} \quad (4)$$

where F is the maximum load. L , b , and h are the span (a distance between supports), width, and thickness of specimens.

4 Application of metallic porous materials

Metallic porous materials or metallic foams are commercially used in various applications according to their physical and mechanical properties. The most important commercial applications of these materials are in the structural (e.g., wear-resistant tools and biomedical implants) and the functional (e.g., catalyst and heat exchangers) fields, which is dependent on the characteristics of metallic porous materials such as morphology, metallurgy, processing, and economy.

4.1 Structural application of metallic porous materials

4.1.1 Wear-resistant tools

A consistent increase in demand of grinding wheel in the field of machining the difficult-to-machine materials for high strength and toughness materials (e.g., nickel and titanium-based alloys) with high efficiency and precision used in aerospace and automotive industry has been presented in recent years [64–74]. Compared to resin and vitrified bond superabrasive grinding wheel, the prominent characteristics of the metal bond ones, (e.g., high toughness, high wear resistance, and long tool life) make them an ideal option in machining the hard and brittle materials. However, the frequently dressing is required to prevent the clogging of grinding wheel due to their insufficient chip storage capacity and poor self-sharpening [75–83]. Furthermore, the poor machining efficiency and quality to grind the difficult-to-machine materials will be affected by the above reasons [84–86]. On account of the exceptional properties of metallic porous materials, properly designed the structure of metallic porous materials by employing the various types of pore-forming agents can improve the performance of the working layer of grinding wheels [87, 88]. In addition, the porous structure of the outer surfaces results in the formed additional cutting edges and then the empty interiors turn into the temporary shallow storage for grinding chips [89]. Naturally, the pores generated by embedding pore-forming agents play a critical role in grinding processes [90]. Along this line of consideration, properly designed the structure of metallic porous materials by employing various types of pore-forming agents is of vital importance to

achieve high porosity and desired mechanical performance simultaneously.

Recently, the pore-forming agents, i.e., granulated sugar [91], polymethyl methacrylate (PMMA) [92] and butyl carbonate [93] have been employed to obtain the grinding wheel with high porosity. However, the pore characteristics (e.g., shape, size, and distribution) generated with the above pore-forming agents by adopting various removal process (i.e., sintering-dissolution, thermally stimulated decomposition, and thermally melted elimination technique) were always tiny and irregular and then unable to accurately obtain the satisfactory physical property and mechanical performance of grinding wheel with high porosity [94]. The embedded alumina hollow particles (see Fig. 8) as pore-forming agents were put forward to fabricate metallic porous materials by Ding et al. [95]. The high interfacial strength of the stable protecting layers between Cu-Sn-Ti composites and CBN superabrasives, Cu-Sn-Ti composites and alumina hollow particles was investigated. Furthermore, the fabricated porous metal-bonded CBN wheels (as presented in Fig. 9) showed a good grinding performance. Chen et al. [96] evaluated the grinding performance of Cu-Sn-Ti bonded CBN wheels with a bending strength of 60 MPa and 30% porosity by using 0.5-mm-size alumina hollow particles (Fig. 10). The results showed that the grinding forces, specific grinding energy, and temperatures of the porous bonded CBN wheels are lower than that of vitrified bonded CBN wheels. Ma et al. [63] evaluated the microstructures and mechanical properties of the porous Cu-Sn-Ti alumina composites by employing alumina hollow particles. The experimental results displayed that the pore size and distribution could be tailored accurately to fabricate the satisfactory porosity and mechanical properties of the porous Cu-Sn-Ti alumina composites and then the wear-resistant tools by employing the porous Cu-Sn-Ti materials would be obtained.

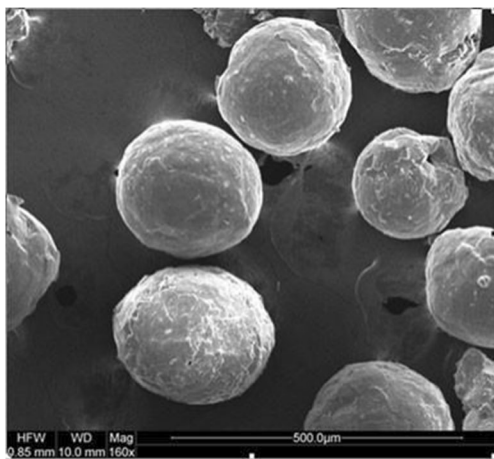


Fig. 8 Morphology of alumina bubble particles with a diameter of 150–250 μm [95]

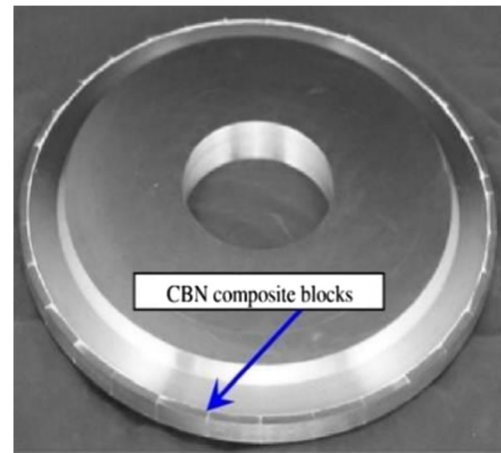


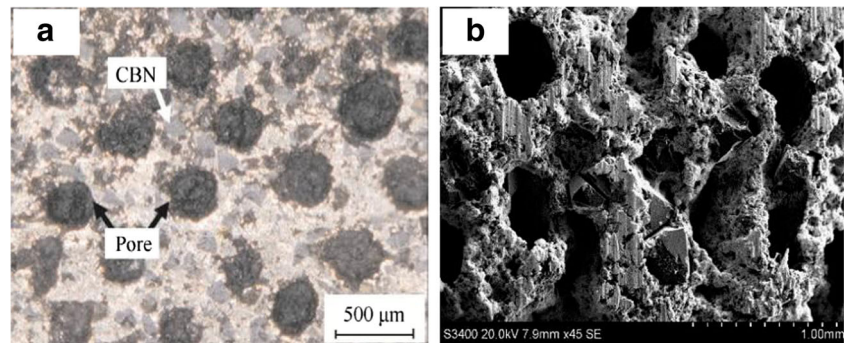
Fig. 9 Porous metal-bonded CBN grinding wheel [95]

4.1.2 Biomedical implants

Metallic materials (e.g., stainless steel, cobalt-chromium alloys, pure Ti and its alloys, and bioactive metallic glass) play a pivotal role as biomaterials to assist with the repair and replacement of natural bones [97–100]. These artificial metallic implants are more applicable for load-bearing applications as compared with ceramics or polymer materials due to their unique combination of high strength and fracture toughness [101, 102]. However, the metallic implants are usually much stiffer as compared to the natural bone represented in Fig. 11a. This mismatch of the Young's modulus can cause stress-shielding effects under load-bearing load potentially leading to bone resorption as shown in Fig. 11b and eventual failure of such implants. Therefore, it is critically important for metallic implants to have well-matching mechanical properties to minimize the stress-shielding effects and their biological properties.

From the biological point of view, the biocompatibility and osteoconductive characteristics of porous materials are closely related to the pore morphology such as size, shape, connectivity, and porosity because of their cell attachment, proliferation, and bond strength between the tissue and the artificial implant in the human body [103–105]. It is well documented that the opened cell porous structure with pore sizes in a range of 50 to 800 μm is suitable for introducing tissue ingrowth which anchors the prosthesis to the surrounding bone and prevents the implant loosening. Moreover, according to the natural bone structure, the porosity of the porous artificial implants should be in range of 30 to 50%, to increase the surface-to volume ratio of the porous materials and, therefore, to promote bone remodeling, cell attachment, growth, and migration [106–108]. From mechanical point of view, the elastic moduli and fracture strength of porous metallic implants should be as close to the human bones. The matching mechanical properties can minimize the stress-shielding effects and prevent the premature failure [109]. From in vivo study, it is confirmed that the

Fig. 10 Morphology of porous bonded CBN wheels. **a** Photograph. **b** SEM micrograph [96]



interconnected metallic porous materials improve the bone ingrowth and interfacial bonding as presented in Table 8 [105–107]. Furthermore, Bandyopadhyay et al. [110] manufactured porous titanium implants with porosities (25%) and evaluated effect of porosity on osteointegration properties in vivo. The distal femur model of male Sprague-Dawley rats was established for a period of 4 and 10 weeks, which was detected with microcomputed tomography. In addition, the strong interfacial bonding between porous titanium implants and the surrounding tissue was closely correlated with porosity at early stage of osseointegration regardless of surface modification. Compared to porous titanium alloys, porous magnesium alloys may be better candidates as biodegradable implants, which can be gradually dissolved and then absorbed or eliminated from body during the stage of convalescence. However, the physical and mechanical properties of porous magnesium alloys as biomedical materials such as poor connectivity and poor corrosion resistance in body's internal environment require further investigation [111]. Porous tantalum alloys as a new developing direction of bone tissue engineering come into sight in view of superior properties such as good biocompatibility, corrosion resistance, bone induction, and regeneration. Though porous tantalum alloys have superior properties, there is still possibility of trouble in mass preparation [112].

4.2 Functional application of metallic porous materials

4.2.1 Catalyst and catalyst carrier

Since the discovery of porous materials attention has been directed to explore their potential applications in catalysis or absorption fields. The mesoporous materials are appropriate for being used not only as acidic, basic, or redox catalysts but also as carriers of highly dispersed metallic or oxidic phases. The mesoporous materials allow the larger molecules to enter the pore system, to be processed there and to leave the pore system again [113, 114]. Liu et al. [115] applied the ordered porous transition metal oxides to remove volatile organic compounds by employing the catalytic combustion method. The resulting catalyst offering excellent catalytic properties such as high reactants interfacial area, low temperature reducibility, and unique porous structure make it a considerable attention as an effective catalyst to eliminate volatile organic compounds. Mikami et al. [116] pointed out that porous Ni materials exhibited high catalytic activity by employing a certain amount of zirconium for the hydrogenation of nitrate in water. In addition, the blockage of porosity could be avoided by employing the element of zirconium and then the porous

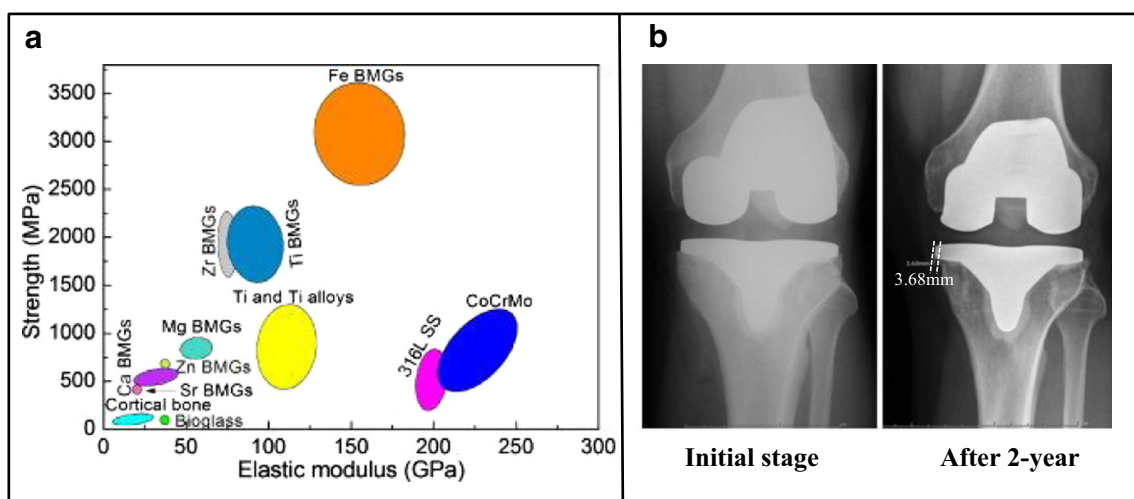
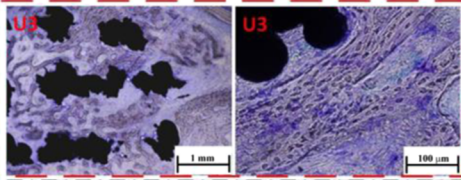
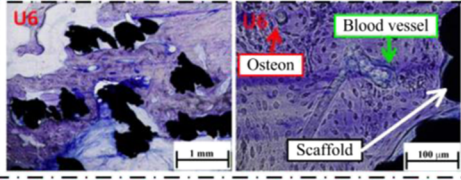

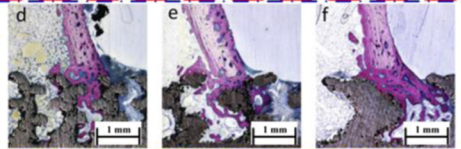
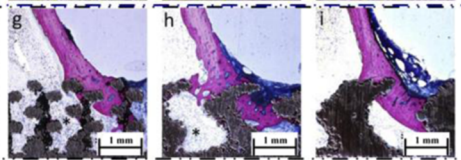
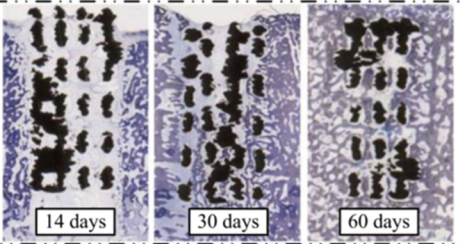
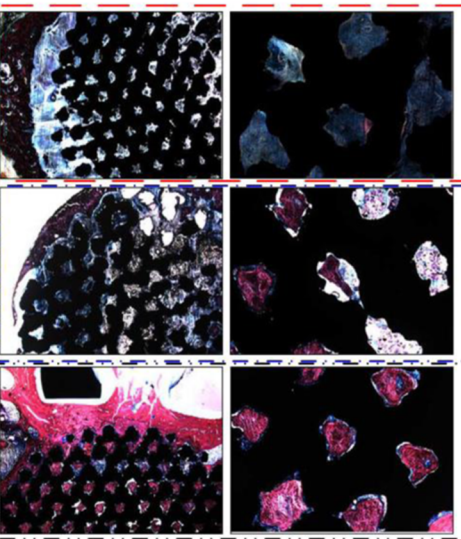


Fig. 11 **a** Mechanical comparisons of metallic alloys and natural bones and **b** stress-shielding effect of cobalt-chromium tibial baseplates [101, 102]

Table 8 Histology images after in vivo study of artificial metallic porous implants [105–107]

No.	Animal model	Implantation site	Duration	Histology	Description
1	Rabbit	Mandibular [78]	3 weeks		After 6 weeks, the amount of bone ingrowth and bone maturity increased.
			6 weeks		
2	Rabbit	Tibia [79]	2 weeks		Purple indicates the bone and silver indicates the titanium implant and marrow like tissue spreading into porous area.
			4 weeks		Pore size increases (300 to 900 μm) from left to right and culture time increases from top to bottom.
			8 weeks		After 8 weeks the new bone has been remodeled into the mature lamellar bone. Marrow-like tissue was evident inside the porous implants.
3	Pig	Frontal skull [80]	14 days		After 14 days only minor bone ingrowth observed in outer region and after 30 days a noticeable growth of osseous tissue discovered in the outer as well as the central regions. However, after 60 days the implants were filled completely with bony tissue.
			30 days		
			60 days		
4	Goat	Metatarsus [81]	3 months		Purple indicates bone; black indicates materials; blue indicates fibrovascular tissue
			6 months		New bone area increased with time and, compared with the middle position, both ends had relatively more amounts of new bone
			12 months		

structure of Ni-based solid catalysts was preserved eventually. Giani et al. [117] investigated the application of the open-porosity metallic materials as catalyst carrier in gas-solid catalytic processes for short periods of contact times and high reaction rates, which typically governed by diffusional mass transport. Furthermore, metallic porous materials have been widely employed to degrade pollutants catalytically.

4.2.2 Heat exchangers

The advanced power system requires higher cooling capability, and the use of opened cell metallic porous materials is one of the suitable ways to increase the heat exchange rate. According to the high surface area to volume ratio, thermal conductivity, and mixing capability of fluids, the metallic porous materials make them effective for the improvement of heat exchanging. A schematic representation is shown in Fig. 12 of the mechanisms by which heat transfer can occur in porous materials [118].

Recently, aluminum- or copper-based porous materials having high conductive and opened cell pores received a special attention as heat exchangers. As has already been stated, the heat transfer performance is largely dependent on the porosity [119, 120], pore size [121, 122], and wall connection [123] of metallic porous materials. Bhattacharya et al. [119] pointed out that the effective thermal conductivity was closely correlated with the porosity of metallic porous materials. Meanwhile, a numerical investigation of porous aluminum materials with high porosity used for air-cooled heat exchangers was

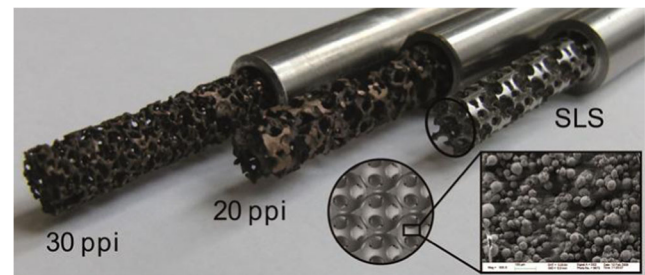


Fig. 13 Comparison of porous metal reactors. Inserted commercial porous elements (20 and 30 ppi) on the left; the fully sintered structure on the right. The SEM image depicts the roughness of the sintered material [125]

elaborated by Ejlali et al. [120]. The results revealed that the heat removal capacity could be improved by applying porous aluminum alloys to a great extent compared to conventional finned design. Boomsma et al. [121] evaluated thermal resistances of heat exchangers fabricated with compressed porous aluminum materials. Results indicated that nearly half of magnitude of thermal resistances was generated with compressed porous aluminum materials compared to the best heat exchanger under same conditions. Furthermore, Mao et al. [122] declared that the heat transfer capability could be strengthened by optimizing the porosity and thickness of porous aluminum alloys. In addition, the convective heat transfer is strongly dependent on the pore size of metallic porous structure [123]. Zhao et al. [124] indicated that the effective thermal conductivity of porous FeCrAlY materials increased with the increasing of pores size (0.1–7 mm) under vacuum condition. Hutter et al.

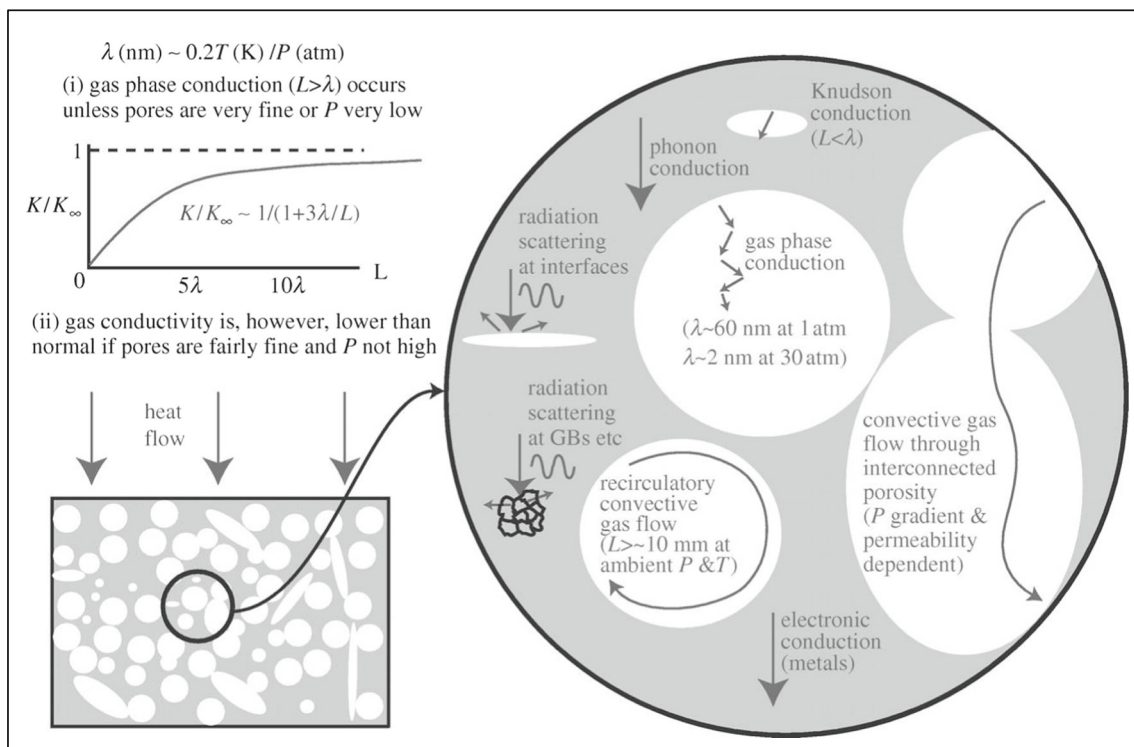


Fig. 12 Mechanisms of heat transfer in porous materials [118]

[125] stated that the pseudo-convective heat transfer rate of the fully sintered structure revealed a 30% increase compared to the sintered structure without wall connection. A comparison morphology of metallic porous reactors between commercially available porous metal reactors and the fully sintered structure is illustrated in Fig. 13.

5 Conclusions and future challenges

This comprehensive review confirmed that the mesoporous and microporous metallic materials are successfully manufactured using various advanced manufacturing processes. Three-dimensional (3D) continuously porous metallic materials are tailored by advanced additives manufacturing (AM) technique. On the other hand, the randomly opened cell or closed cell metallic porous materials are manufactured using powder metallurgy technique. The pore-forming agents are removed by heat treatment or dissolving processes without leaving identifiable processing defects (e.g., formation of a second phase, delamination, and cracks). The irregular shapes pores are distributed throughout the final structure. However, the pore morphologies for example pore size, shape, porosity, and connectivity rely on the physical behavior and volume percentage of pore-forming agents. It is noticeable that the porosity in metallic porous materials negatively impact on their mechanical properties.

Although there are great progresses in manufacturing process of metallic porous materials, there are still significant challenges:

- (1) The pore morphologies depending on various factors (e.g., pore-forming agent types, size, shape and prices, the removal process, and the sintering technology) have a great influence on the microstructure and/or mechanical properties of metallic porous materials. A partially ordered arrangement of the pores has been achieved in previous studies. However, the uniformity of the pores in final whole structure needs to be studied further.
- (2) Though the parametric investigations with the sintering process, porosity, and fabrication technology have been studied, there is no practicable theoretical and numerical model to estimate the influence of various parameters on the microstructure and mechanical properties.
- (3) A wide-ranging applications in structural (wear-resistant tools and biomedical implants, etc.) and the functional (catalyst and heat exchangers, etc.) aspects of metallic porous materials have been discussed. However, their highly manufacturing cost minimized their application area. Therefore, it is necessary to establish a cost-effective manufacturing technique that can match the physical and mechanical properties of metallic porous materials for advanced industrial applications.

Acknowledgements This work is financially supported by the National Natural Science Foundation of China (No. 51775275 and No. 51375235) and the Fundamental Research Funds for the Central Universities (No. NE2014103 and No. NZ2016107).

References

1. Perego C, Millini R (2013) Porous materials in catalysis: challenges for mesoporous materials. *Chem Soc Rev* 42(9):3956–3976. <https://doi.org/10.1039/C2CS35244C>
2. Mentz J, Krone L, Bram M, Buchkremer HP, Stover D (2006) Using MIM to make porous implants with shape memory. *Metal Powder Report* 61:20–25
3. Banhart J (2001) Manufacture, characterization and application of cellular metals and metal foams. *Prog Mater Sci* 46(6):559–632. [https://doi.org/10.1016/S0079-6425\(00\)00002-5](https://doi.org/10.1016/S0079-6425(00)00002-5)
4. Xie ZK, Diologent F, Salvo L, Mortensen A (2004) Sound absorption characteristics of lotus-type porous copper fabricated by unidirectional solidification. *Mater Sci Eng A* 386(1–2):390–395. [https://doi.org/10.1016/S0921-5093\(04\)00966-9](https://doi.org/10.1016/S0921-5093(04)00966-9)
5. Dunand DC (2004) Processing of titanium foams. *Adv Eng Mater* 6(6):369–376. <https://doi.org/10.1002/adem.200405576>
6. Cai Y, Li X, Dong J (2014) Microstructure and mechanical properties of porous Si₃N₄-SiO₂ ceramics fabricated by a process combining carbothermal reduction and sol-gel infiltration-sintering. *Mater Sci Eng A* 601(8):111–115. <https://doi.org/10.1016/j.msea.2014.01.087>
7. Hou Z, Ye F, Liu L, Liu Q (2012) Fabrication of gradient porous β-SiAlON ceramics via a camphene-based freeze casting process. *Mater Sci Eng A* 558:742–746. <https://doi.org/10.1016/j.msea.2012.08.094>
8. Cruz HS, Spino J, Grathwohl G (2008) Nanocrystalline ZrO₂ ceramics with idealized macropores. *Journal of European Ceramic Society* 28(9):1783–1791
9. Kishimoto A, Okada M, Teranishi T, Hayashi H (2013) Maintaining the mechanical strength of La-,Y-co- substituted zirconia porous ceramics through the super plastically foaming method. *Mater Sci Eng A* 581(10):98–103. <https://doi.org/10.1016/j.msea.2013.05.084>
10. Lazinska M, Durejko T, Lipniski S, Polkowski W, Czujko T, Varin RA (2015) Porous graded FeAl intermetallic foams fabricated by sintering process using NaCl space holders. *Mater Sci Eng A* 636:407–414. <https://doi.org/10.1016/j.msea.2015.02.053>
11. Wang X, Xu S, Zhou S, Xu W, Leary M, Choong P, Qian M, Brandt M, Xie YM (2016) Topological design and additive manufacturing of porous metals for bone scaffolds and orthopaedic implants: a review. *Biomaterials* 83:127–141. <https://doi.org/10.1016/j.biomaterials.2016.01.012>
12. Gaillard C, Despois JF, Mortensen A (2004) Processing of NaCl powders of controlled size and shape for the microstructural tailoring of aluminium foams. *Mater Sci Eng A* 374(1–2):250–262. <https://doi.org/10.1016/j.msea.2004.03.015>
13. Gain AK, Zhang LC, Liu WD (2015) Microstructure and material properties of porous hydroxyapatite-zirconia nanocomposites using polymethyl methacrylate powders. *Mater Des* 67:136–144. <https://doi.org/10.1016/j.matdes.2014.11.028>
14. Aydoğmuş T, Bor Ş (2009) Processing of porous TiNi alloys using magnesium as space holder. *J Alloys Compd* 478(1–2):705–710. <https://doi.org/10.1016/j.jallcom.2008.11.141>
15. Vogiatzis CA, Tsouknidas A, Kountouras DT, Skolianos S (2015) Aluminum-ceramic cenospheres syntactic foams produced by powder metallurgy route. *Mater Des* 85:444–454. <https://doi.org/10.1016/j.matdes.2015.06.154>

16. Son BH, Hong JG, Hyun YT, Bae SC, Kim SE (2012) A study on pore structure and mechanical properties of porous titanium fabricated by three-dimensional layer manufacturing process. *Korean J Metals Materials* 50(2):100–106
17. Sobczak JJ, Drenchev L (2013) Metallic functionally graded materials: a specific class of advanced composites. *J Mater Sci Technol* 29(4):297–316. <https://doi.org/10.1016/j.jmst.2013.02.006>
18. IH O, Nomura N, Masahashi N, Hanada S (2003) Mechanical properties of porous titanium compacts prepared by powder sintering. *Scr Mater* 49(12):1197–1202
19. Zdravkov BD, Cermak JJ, Sefara M, Jank J (2007) Pore classification in the characterization of porous materials: a perspective. *Cent Eur J Chem* 5(2):385–395
20. Kasemset S, Wang L, He ZW, Miller DJ, Kirschner A, Freeman BD, Sharma MM (2017) Influence of polydopamine deposition conditions on hydraulic permeability, sieving coefficients, pore size and pore size distribution for a polysulfone ultrafiltration membrane. *J Membr Sci* 552(15):100–115
21. Wang QZ, Cui CX, Liu SJ, Zhao LC (2010) Open-celled porous Cu prepared by replication of NaCl space-holders. *Mater Sci Eng A* 527(4–5):1275–1278. <https://doi.org/10.1016/j.msea.2009.10.062>
22. Golabgir MH, Ebrahimi-Kahrizsangi R, Torabi O, Tajizadegan H, Jamshidi A (2014) Fabrication and evaluation of oxidation resistance performance of open-celled Fe(Al) foam by space-holder technique. *Adv Powder Technol* 25(3):960–967. <https://doi.org/10.1016/j.apt.2014.01.020>
23. Jha N, Mondal DP, Majumdar JD, Badkul A, Jha AK, Khare AK (2013) Highly porous open cell Ti-foam using NaCl as temporary space holder through powder metallurgy route. *Mater Des* 47: 810–819. <https://doi.org/10.1016/j.matdes.2013.01.005>
24. Zhao XK, Sun HB, Lan L, Huang JH, Zhang H, Wang Y (2009) Pore structures of high-porosity NiTi alloys made from elemental powders with NaCl temporary space-holders. *Mater Lett* 63(28): 2402–2404. <https://doi.org/10.1016/j.matlet.2009.07.069>
25. Bakan HI (2006) A novel water leaching and sintering process for manufacturing highly porous stainless steel. *Scr Mater* 55(2):203–206. <https://doi.org/10.1016/j.scriptamat.2006.03.039>
26. Bafti H, Habibolahzadeh A (2010) Production of aluminum foam by spherical carbamide space holder technique-processing parameters. *Mater Des* 31(9):4122–4129. <https://doi.org/10.1016/j.matdes.2010.04.038>
27. Michailidis N, Stergioudi F, Tsouknidas A, Pavlidou E (2011) Compressive response of Al-foams produced via a powder sintering process based on a leachable space-holder material. *Mater Sci Eng A* 528(3):1662–1667. <https://doi.org/10.1016/j.msea.2010.10.088>
28. Jakubowicz J, Adamek G, Pałka K, Andrzejewski D (2015) Micro-CT analysis and mechanical properties of Ti spherical and polyhedral void composites made with saccharose as a space holder material. *Mater Charact* 100(100):13–20. <https://doi.org/10.1016/j.matchar.2014.12.006>
29. Gülsoy HÖ, German RM (2008) Production of micro-porous austenitic stainless steel by powder injection molding. *Scr Mater* 58(4):295–298. <https://doi.org/10.1016/j.scriptamat.2007.10.004>
30. Xie ZK, Yamada YS, Banno T (2007) Fabrication of micro porous aluminum by powder sintering. *Mater Sci Forum* 539(3):2778–2781
31. Hsu HC, SC W, Hsu SK, Tsai MS, Chang TY, Ho WF (2013) Processing and mechanical properties of porous Ti-7.5Mo alloy. *Mater Des* 47:21–26. <https://doi.org/10.1016/j.matdes.2012.12.043>
32. Luo HJ, Lin H, Chen PH, Yao GC (2015) Decomposition behavior of titanium hydride treated by surface oxidation. *Rare Metals* 34(1):28–33. <https://doi.org/10.1007/s12598-014-0415-z>
33. Ahn MK, Jo IH, Koh YH, Kim HE (2014) Production of highly porous titanium (Ti) scaffolds by vacuum-assisted foaming of titanium hydride (TiH₂) suspension. *Mater Lett* 120(2):228–231. <https://doi.org/10.1016/j.matlet.2014.01.065>
34. Gain AK, Zhang L, Quadir MZ (2016) Composites matching the properties of human cortical bones: the design of porous titanium-zirconia (Ti-ZrO₂) nanocomposites using polymethyl methacrylate powders. *Mater Sci Eng A* 662:258–267. <https://doi.org/10.1016/j.msea.2016.03.066>
35. Aşik EE, Bor Ş (2015) Fatigue behavior of Ti-6Al-4V foams processed by magnesium space holder technique. *Mater Sci Eng A* 621:157–165. <https://doi.org/10.1016/j.msea.2014.10.068>
36. Chino Y, Dunand DC (2008) Directionally freeze-cast titanium foam with aligned, elongated pores. *Acta Mater* 56(1):105–113. <https://doi.org/10.1016/j.actamat.2007.09.002>
37. Guo RQ, Rohatgi PK (1997) Preparation of aluminium-fly ash particulate composite by powder metallurgy technique. *J Mater Sci* 32(15):3971–3974. <https://doi.org/10.1023/A:1018625118090>
38. Rheinheimer V, YP W, Wu T, Celik K, Wang JY, Lorenzis LD, Wriggers P, Zhang MH, Monteiro PJ (2017) Multi-scale study of high-strength low-thermal-conductivity cement composites containing cenospheres. *Cem Concr Compos* 80:91–103. <https://doi.org/10.1016/j.cemconcomp.2017.03.002>
39. Vogiatzis CA, Skolianos SM (2016) On the sintering mechanisms and microstructure of aluminium-ceramic cenospheres syntactic foams produced by powder metallurgy route. *Compos Part A* 82:8–19. <https://doi.org/10.1016/j.compositesa.2015.11.037>
40. Parthasarathya J, Starlya B, Ramana S, Christensen A (2010) Mechanical evaluation of porous titanium (Ti6Al4V) structures with electron beam melting (EBM). *J Mechanical Behavior Biomedical Materials* 3(3):249–259. <https://doi.org/10.1016/j.jmbbm.2009.10.006>
41. Heinel P, Muller L, Komer C, Singer RF, Muller FA (2008) Cellular Ti-6Al-4V structures with interconnected macro porosity for bone implants fabricated by selective electron beam melting. *Acta Biomater* 4(5):1536–1544. <https://doi.org/10.1016/j.actbio.2008.03.013>
42. Parthasarathya J, Starlya B, Ramana SA (2011) Design for the additive manufacture of functionally graded porous structures with tailored mechanical properties for biomedical applications. *J Manuf Process* 13(2):160–170. <https://doi.org/10.1016/j.jmapro.2011.01.004>
43. Wen CE, Mabuchi M, Yamada Y, Shimojima K, Chino Y, Asahina T (2001) Processing of biocompatible porous Ti and Mg. *Scr Mater* 45(10):1147–1153. [https://doi.org/10.1016/S1359-6462\(01\)01132-0](https://doi.org/10.1016/S1359-6462(01)01132-0)
44. Raj RE, Daniel BSS (2009) Structural and compressive property correlation of closed-cell aluminum foam. *J Alloys Compd* 467(1–2):550–556. <https://doi.org/10.1016/j.jallcom.2007.12.040>
45. Jiang B, Zhao NQ, Shi CS, Li JJ (2005) Processing of open cell aluminum foams with tailored porous morphology. *Scr Mater* 53(6):781–785. <https://doi.org/10.1016/j.scriptamat.2005.04.055>
46. Nieh TG, Higashi K, Wadsworth J (2000) Effect of cell morphology on the compressive properties of open-cell aluminum foams. *Mater Sci Eng A* 283(1–2):105–110. [https://doi.org/10.1016/S0921-5093\(00\)00623-7](https://doi.org/10.1016/S0921-5093(00)00623-7)
47. Bafti H, Habibolahzadeh A (2013) Compressive properties of aluminum foam produced by powder-Carbamide spacer route. *Mater Des* 52(24):404–411. <https://doi.org/10.1016/j.matdes.2013.05.043>
48. Imwinkelried T (2007) Mechanical properties of open-pore titanium foam. *J Biomed Mater Res A* 81(4):964–970. <https://doi.org/10.1002/jbm.a.31118>
49. Tuncer N, Arslan G, Maire E, Salvo L (2011) Influence of cell aspect ratio on architecture and compressive strength of titanium

- foams. *Mater Sci Eng A* 528(24):7368–7374. <https://doi.org/10.1016/j.msea.2011.06.028>
50. Gao ZF, Li QY, He F, Huang Y, Wan YZ (2012) Mechanical modulation and bioactive surface modification of porous Ti-10Mo alloy for bone implants. *Mater Des* 42:13–20. <https://doi.org/10.1016/j.matdes.2012.05.041>
 51. Wang QZ, DM L, Cui CX, Liang LM (2011) Compressive behaviors and energy-absorption properties of an open-celled porous Cu fabricated by replication of NaCl space-holders. *J Mater Process Technol* 211(3):363–367. <https://doi.org/10.1016/j.jmatprotec.2010.10.008>
 52. Nakaş Gİ, Dericioğlu AF (2011) Bor Ş. Fatigue behavior of TiNi foams processed by the magnesium space holder technique. *J Mechanical Behavior of Biomed Mater* 4:2017–2023
 53. Li JC, Dunand DC (2011) Mechanical properties of directionally freeze-cast titanium foams. *Acta Mater* 59(1):146–158. <https://doi.org/10.1016/j.actamat.2010.09.019>
 54. Sankaranarayanan S, Nguyen QB, Shabadi R, Almajid AH, Gupta M (2016) Powder metallurgy hollow fly ash cenospheres' particles reinforced magnesium composites. *Powder Metall* 59(3):188–196. <https://doi.org/10.1080/00325899.2016.1139339>
 55. Vogiatzis CA, Tsouknidas A, Kountouras DT, Skolianos S (2015) Aluminum-ceramic cenospheres syntactic foams produced by powder metallurgy route. *Mater Des* 85:444–454. <https://doi.org/10.1016/j.matdes.2015.06.154>
 56. Mediaswanti K, Wen C, Ivanova EP, Berndt CC, Malherbe F, Hong Pham VT, Wang JA (2013) Review on bioactive porous metallic biomaterials. *J Biomimetics Biomaterials Tissue Eng* 18:1–8
 57. Niu W, Gill S, Dong H, Bai CA (2010) Two-scale model for predicting elastic properties of porous titanium formed with space-holders. *Comput Mater Sci* 50(1):172–178. <https://doi.org/10.1016/j.commatsci.2010.07.022>
 58. Barrabés M, Sevilla P, Planell JA, Gil FJ (2008) Mechanical properties of nickel-titanium foams for reconstructive orthopaedics. *Mater Sci Eng C* 28(1):23–27. <https://doi.org/10.1016/j.msec.2007.02.001>
 59. Eggeler G, Hornbogen E, Yawny A, Heckmann A, Wagner M (2004) Structural and functional fatigue of NiTi shape memory alloys. *Mater Sci Eng A* 378(1-2):24–33. <https://doi.org/10.1016/j.msea.2003.10.327>
 60. Lin JG, Zhang YF, Ma M (2010) Preparation of porous Ti35Nb alloy and its mechanical properties under monotonic and cyclic loading. *Trans Nonferrous Metals Soc China* 20(3):390–394. [https://doi.org/10.1016/S1003-6326\(09\)60151-5](https://doi.org/10.1016/S1003-6326(09)60151-5)
 61. Zetl B, Mayer H, Stanzl-Tschegg SE, Degischer HP (2000) Fatigue properties of aluminum foams at high numbers of cycles. *Mater Sci Eng A* 292(1):1–7. [https://doi.org/10.1016/S0921-5093\(00\)01033-9](https://doi.org/10.1016/S0921-5093(00)01033-9)
 62. Amigó V, Reig L, Busquets DJ, Ortiz JL, Calero JA (2011) Analysis of bending strength of porous titanium processed by space holder method. *Powder Metall* 54(1):67–70. <https://doi.org/10.1179/174329009X409697>
 63. Ma CY, Ding WF, JH X, Fu YC (2015) Influence of alumina bubble particles on microstructure and mechanical strength in porous Cu-Sn-Ti metals. *Mater Des* 65:50–56. <https://doi.org/10.1016/j.matdes.2014.09.002>
 64. Kopac J, Krajnik P (2006) High-performance grinding—a review. *J Mater Process Technol* 175(1-3):278–284. <https://doi.org/10.1016/j.jmatprotec.2005.04.010>
 65. Zhang ZY, Guo DM, Kang RK, Gao H, Jin ZJ, Meng YW (2010) Subsurface crystal lattice deformation machined by ultraprecision grinding of soft-brittle CdZnTe crystals. *Int J Adv Manuf Technol* 47(9-12):1065–1081. <https://doi.org/10.1007/s00170-009-2253-y>
 66. Mao C, Zhou X, Yin LR, Zhang MJ, Tang K, Zhang J (2016) Investigation of the flow field for a double-outlet nozzle during minimum quantity lubrication grinding. *Int J Adv Manuf Technol* 85(1-4):291–298. <https://doi.org/10.1007/s00170-015-7896-2>
 67. Li CH, Zhao HY, Ma HL, Hou YL, Zhang YB, Yang M, Zhang XW (2015) Simulation study on effect of cutting parameters and cooling mode on bone-drilling temperature field of superhard drill. *Int J Adv Manuf Technol* 81(9-12):2027–2038. <https://doi.org/10.1007/s00170-015-7259-z>
 68. Ding WF, Zhang LC, Li Z, Zhu YJ, HH S, Xu JH (2017) Review on grinding-induced residual stresses in metallic materials. *Int J Adv Manuf Technol* 88(9-12):2939–2968. <https://doi.org/10.1007/s00170-016-8998-1>
 69. Zhang ZY, Meng YW, Guo DM, Kang RK, Gao H (2010) Nanoscale machinability and subsurface damage machined by CMP of soft-brittle CdZnTe crystals. *Int J Adv Manuf Technol* 47(9-12):1105–1112. <https://doi.org/10.1007/s00170-009-2225-2>
 70. Mao C, Ren YH, Gan HY, Zhang MJ, Zhang J, Tang K (2015) Microstructure and mechanical properties of cBN-WC-Co composites used for cutting tools. *Int J Adv Manuf Technol* 76(9-12):2043–2049. <https://doi.org/10.1007/s00170-014-6410-6>
 71. Zhang YB, Li CH, Zhang Q, Jia DZ, Wang S, Zhang DK, Mao C (2016) Improvement of useful flow rate of grinding fluid with simulation schemes. *Int J Adv Manuf Technol* 84(9-12):2113–2126. <https://doi.org/10.1007/s00170-015-7864-x>
 72. He ZB, Huang H, Yin F, Xu XP (2017) Development of a brazed diamond wire for slicing single-crystal sic ingots. *Int J Adv Manuf Technol* 91(1-4):189–199. <https://doi.org/10.1007/s00170-016-9750-6>
 73. Huang H, Zhang Y, Xu X (2015) Experimental investigation on the machining characteristics of single-crystal sic sawing with the fixed diamond wire. *Int J Adv Manuf Technol* 81(5-8):955–965. <https://doi.org/10.1007/s00170-015-7250-8>
 74. Chandra A, Bastawros AF, TY Y, Asplund DT (2017) Chemical mechanical paired grinding: a tool for multi-wavelength planarization. *Int J Adv Manuf Technol* 89(1-4):611–617. <https://doi.org/10.1007/s00170-016-9085-3>
 75. Yu TY, Bastawros AF, Chandra A. Experimental characterization of electroplated CBN grinding wheel wear: topology evolution and interfacial toughness. Proceedings of the ASME 9th International Manufacturing Science and Engineering Conference, Detroit MI. Jun 9–13, 2014
 76. Ding WF, Dai CW, TY Y, JH X, Fu YC (2017) Grinding performance of textured monolayer CBN wheels: undeformed chip thickness nonuniformity modeling and ground surface topography prediction. *Int J Mach Tools Manuf* 122:66–80. <https://doi.org/10.1016/j.ijmachtools.2017.05.006>
 77. TY Y, Asplund DT, Bastawros AF, Chandra A (2016) Performance and modeling of paired polishing process. *Int J Mach Tools Manuf* 109:49–57
 78. Zhu YJ, Ding WF, Yu TY, Xu JH, Fu YC, Su HH (2017) Investigation on stress distribution and wear behavior of brazed polycrystalline cubic boron nitride superabrasive grains: numerical simulation and experimental study. *Wear* 376-377:1234–1244. <https://doi.org/10.1016/j.wear.2016.12.048>
 79. Ding WF, Li HN, Zhang LC, JH X, YC F, Su HH (2017) Diamond wheel dressing: a comprehensive review. *ASME J Manufacturing Sci Engineering* 139(12):121006. <https://doi.org/10.1115/1.4037991>
 80. Dai CW, Ding WF, JH X, YC F, Yu TY (2017) Influence of grain wear on material removal behavior during grinding nickel-based superalloy with a single diamond grain. *Int J Mach Tools Manuf* 113:49–58. <https://doi.org/10.1016/j.ijmachtools.2016.12.001>
 81. TY Y, Bastawros AF, Chandra A (2017) Experimental and modeling characterization of wear and life expectancy of electroplated CBN grinding wheels. *Int J Mach Tools Manuf* 121:70–80
 82. Li Z, Ding WF, Shen L, Xi XX, Fu YC (2016) Comparative investigation on high-speed grinding of TiCp/Ti-6Al-4V

- particulate reinforced titanium matrix composites with single-layer electroplated and brazed CBN wheels. *Chin J Aeronaut* 29(5):1414–1424. <https://doi.org/10.1016/j.cja.2016.01.005>
83. Ding WF, Linke B, Zhu YJ, Li Z, YC F, HH S, Xu JH (2017) Review on monolayer CBN superabrasive wheels for grinding metallic materials. *Chin J Aeronaut* 30(1):109–134. <https://doi.org/10.1016/j.cja.2016.07.003>
 84. Zhu YJ, Ding WF, JH X, Yang CY (2015) An investigation of residual stresses in brazed cubic boron nitride abrasive grains by finite element modelling and Raman spectroscopy. *Mater Des* 87:342–351. <https://doi.org/10.1016/j.matdes.2015.08.039>
 85. Zhao B, Ding WF, JH X, Su HH (2016) Comparative study on cutting behavior of vitrified cubic boron nitride wheel and electroplated cubic boron nitride wheel in high-speed grinding of (TiCp+TiBw)/Ti-6Al-4V composites. Proceedings of the Institution Of Mechanical Engineering, Part B. *J Eng Manuf* 230(3):428–438. <https://doi.org/10.1177/0954405414553457>
 86. Ding WF, Zhu YJ, Zhang LC, Xu JH, Fu YC, Liu WD, Yang CY (2015) Stress characteristics and fracture wear of brazed CBN grains in monolayer grinding wheels. *Wear* 332–333:800–809. <https://doi.org/10.1016/j.wear.2014.12.008>
 87. Zhao B, TY Y, Ding WF, Li XY (2017) Effects of pore structure and distribution on strength of porous Cu-Sn-Ti alumina composites. *Chin J Aeronaut*. <https://doi.org/10.1016/j.cja.2017.08.008>
 88. Kurgan N (2014) Effect of porosity and density on the mechanical and microstructural properties of sintered 316L stainless steel implant materials. *Material Design* 55:235–241. <https://doi.org/10.1016/j.matdes.2013.09.058>
 89. HH S, HJ X, Xiao B, YC F, Xu JH (2006) Microstructure and performance of porous Ni-Cr alloy bonded diamond grinding wheel. *Mater Sci Forum* 532:373–376
 90. Dai QL, Luo CB, Liao CJ (2008) Experimental study on porous metal bonded diamond grinding wheels (II)-grinding performance of porous wheels. *Key Eng Mater* 359:48–52
 91. Mao JB, Zhang FL, Liao GC, Zhou YM, Huang HP, Wang CY, Wu SH (2014) Effect of granulated sugar as pore former on the microstructure and mechanical properties of the vitrified bond cubic boron nitride grinding wheels. *Mater Des* 60:328–333. <https://doi.org/10.1016/j.matdes.2014.04.006>
 92. Lv XF, Li ZH, Zhu TM, Zhao JS, Zhao GT (2013) Effect of PMMA pore former on microstructure and mechanical properties of vitrified bond CBN grinding wheels. *Ceram Int* 39(2):1893–1899. <https://doi.org/10.1016/j.ceramint.2012.08.038>
 93. Davis TD, Sheldon D, Erkey C (2005) Highly porous vitrified bonded abrasives by the selective extraction of butyl carbonate from green grinding wheels with supercritical CO₂. *J Am Ceram Soc* 88(7):1729–1733. <https://doi.org/10.1111/j.1551-2916.2005.00276.x>
 94. Tomino H, Tsukuda A, Kondo Y (1999) Influence of porosity on grinding performance of porous cast-iron bonded diamond grinding wheel made by pulse current sintering method. *Journal of the Japan Society of Powder and. Powder Metall* 46(3):257–261
 95. Ding WF, JH X, Chen ZZ, Yang CY, Song CJ, Fu YC (2013) Fabrication and performance of porous metal-bonded CBN grinding wheels using alumina bubble particles as pore-forming agents. *Int J Adv Manuf Technol* 67(5–8):1309–1315. <https://doi.org/10.1007/s00170-012-4567-4>
 96. Chen ZZ, JH X, Ding WF, Ma CY (2014) Grinding performance evaluation of porous composite-bonded CBN wheels for Inconel 718. *Chin J Aeronaut* 27(4):1022–1029
 97. Bauer S, Schmuki P, Mark KVD, Park J (2013) Engineering bio-compatible implant surfaces part I: materials and surfaces. *Prog Mater Sci* 58(3):261–326. <https://doi.org/10.1016/j.pmatsci.2012.09.001>
 98. Zhang Y, Hansen HN, Tang PT, Nielsen JS (2013) Verification of a characterization method of the laser-induced selective activation based on industrial lasers. *Int J Adv Manuf Technol* 68(5-8):1775–1783. <https://doi.org/10.1007/s00170-013-4975-0>
 99. Song XH, Wei L, Song PH, QY S, Wei QS, Shi YS, Liu K, Liu WG (2015) Selective laser sintering of aliphatic-polycarbonate/hydroxyapatite composite scaffolds for medical applications. *Int J Adv Manuf Technol* 81:15–25
 100. Li HF, Zheng YF (2016) Recent advances in bulk metallic glasses for biomedical applications. *Acta Biomater* 36:1–20. <https://doi.org/10.1016/j.actbio.2016.03.047>
 101. Martin JR, Watts CD, Levy DL, Kim RH (2017) Medial tibial stress shielding: a limitation of cobalt chromium tibial baseplates. *J Arthroplast* 32(2):558–562. <https://doi.org/10.1016/j.arth.2016.07.027>
 102. Cao H, Feng L, Wu Z, Hou W, Li S, Hao Y, Wu L (2017) Effect of low-intensity pulsed ultrasound on the biological behavior of osteoblasts on porous titanium alloy scaffolds: an in vitro and in vivo study. *Mater Sci Eng C* 80:7–17. <https://doi.org/10.1016/j.msec.2017.05.078>
 103. Zarroug A, Bouznif Z, Hamed ZB, Derbali L, Ezzaouia H (2017) Optoelectronic effect of porous silicon surface treatment with samarium ions for different deposition times and characterizations. *Int J Adv Manuf Technol* 93(5-8):2403–2410. <https://doi.org/10.1007/s00170-017-0600-y>
 104. Dan L, Radu SA, Frătilă D, Berce P (2015) Studies on design of customized orthopedic endoprostheses of titanium alloy manufactured by SLM. *Int J Adv Manuf Technol* 79:905–920
 105. Kundakcioglu E, Lazoglu I, Rawal S (2016) Transient thermal modeling of laser-based additive manufacturing for 3D freeform structures. *Int J Adv Manuf Technol* 85(1-4):493–501. <https://doi.org/10.1007/s00170-015-7932-2>
 106. Taniguchi N, Fujibayashi S, Takemoto M, Sasaki K, Otsuki B, Nakamura T, Matsushita T, Kokubo T, Matsuda S (2016) Effect of pore size on bone ingrowth into porous titanium implants fabricated by additive manufacturing: an in vivo experiment. *Mater Sci Eng C* 59:690–701. <https://doi.org/10.1016/j.msec.2015.10.069>
 107. Ponader S, Wilmowsky CV, Widenmayer M, Lutz R, Heintz P, Korner C, Singer RF, Nkenke E, Neukam FW, Schlegel KA (2010) In vivo performance of selective electron beam-melted Ti-6Al-4V structures. *J Biomed Mater Res A* 92(1):56–62. <https://doi.org/10.1002/jbm.a.32337>
 108. Li G, Wang L, Pan W, Yang F, Jiang W, Wu X, Kong X, Dai K, Hao Y (2016) *In vitro* and *in vivo* study of additive manufactured porous Ti6Al4V scaffolds for repairing bone defects. *Sci Rep* 6:1–11
 109. Ryan G, Pandit A, Apatsidis DP (2006) Fabrication methods of porous metals for use in orthopaedic applications. *Biomaterials* 27(13):2651–2670. <https://doi.org/10.1016/j.biomaterials.2005.12.002>
 110. Bandyopadhyay A, Shivaram A, Tarafder S, Sahasrabudhe H, Banerjee D, Bose S (2017) In vivo response of laser processed porous titanium implants for load-bearing implants. *Ann Biomed Eng* 45(1):249–260. <https://doi.org/10.1007/s10439-016-1673-8>
 111. Trinidad J, Marco I, Arruebarrena G, Wendt J, Letzig D, Saenz de Argandona E, Goodall R (2014) Processing of magnesium porous structures by infiltration casting for biomedical applications. *Adv Eng Mater* 16(2):241–247. <https://doi.org/10.1002/adem.201300236>
 112. Balla VK, Bodhak S, Bose S, Bandyopadhyay A (2010) Porous tantalum structures for bone implants: fabrication, mechanical and in vitro biological properties. *Acta Biomater* 6(8):3349–3359. <https://doi.org/10.1016/j.actbio.2010.01.046>
 113. Perego C, Millini R (2013) Porous materials in catalysis: challenges for mesoporous materials. *Chem Soc Rev* 42(9):3956–3976. <https://doi.org/10.1039/C2CS35244C>

114. Taguchi A, Schuth F (2005) Ordered mesoporous materials in catalysis. *Microporous Mesoporous Mater* 77(1):1–45. <https://doi.org/10.1016/j.micromeso.2004.06.030>
115. Liu YX, Deng JG, Xie SH, Wang ZW, Dai HX (2016) Catalytic removal of volatile organic compounds using ordered porous transition metal oxide and supported noble metal catalysts. *Chin J Catal* 37(8):1193–1205. [https://doi.org/10.1016/S1872-2067\(16\)62457-9](https://doi.org/10.1016/S1872-2067(16)62457-9)
116. Mikami I, Yoshinaga Y, Okuhara T (2004) Rapid removal of nitrate in water by hydrogenation to ammonia with Zr-modified porous Ni catalysts. *Appl Catal B Environ* 49(3):173–179. <https://doi.org/10.1016/j.apcatb.2003.12.009>
117. Giani L, Groppi G, Tronconi E (2005) Heat transfer characterization of metallic foams. *Ind Eng Chem Res* 44(24):9078–9085. <https://doi.org/10.1021/ie050598p>
118. Clyne TW, Golosnoy IO, Tan JC, Markaki AE (2006) Porous materials for thermal management under extreme conditions. *Phil Trans R Soc A* 364(1838):125–146. <https://doi.org/10.1098/rsta.2005.1682>
119. Bhattacharya A, Calmidi VV, Mahajan RL (2002) Thermophysical properties of high porosity metal foams. *Int J Heat Mass Transf* 45(5):1017–1031. [https://doi.org/10.1016/S0017-9310\(01\)00220-4](https://doi.org/10.1016/S0017-9310(01)00220-4)
120. Ejlali A, Ejlali A, Hooman K, Gurgenci H (2009) Application of high porosity metal foams as air-cooled heat exchangers to high heat load removal systems. *Int Communications Heat Mass Transfer* 36(7):674–679. <https://doi.org/10.1016/j.icheatmasstransfer.2009.03.001>
121. Boomsma K, Poulidakos D, Zwick F (2003) Metal foams as compact high performance heat exchangers. *Mech Mater* 35(12):1161–1176. <https://doi.org/10.1016/j.mechmat.2003.02.001>
122. Mao SL, Love N, Leanos A, Rodriguez-Melo G (2014) Correlation studies of hydrodynamics and heat transfer in metal foam heat exchangers. *Appl Therm Eng* 71(1):104–118. <https://doi.org/10.1016/j.applthermaleng.2014.06.035>
123. Bhattacharya A, Mahajan RL (2006) Metal foam and finned metal foam heat sinks for electronics cooling in buoyancy-induced convection. *J Electron Packag* 128(3):259–266. <https://doi.org/10.1115/1.2229225>
124. Zhao CY, TJ L, Hodson HP, Jackson JD (2004) The temperature dependence of effective thermal conductivity of open-celled steel alloy foams. *Mater Sci Eng A* 367(1-2):123–131. <https://doi.org/10.1016/j.msea.2003.10.241>
125. Hutter C, Büchi D, Zuber V, Rudolf von Rohr P (2011) Heat transfer in metal foams and designed porous media. *Chem Eng Sci* 66(17):3806–3814. <https://doi.org/10.1016/j.ces.2011.05.005>